Korean J. Chem. Eng., 39(1), 146-160 (2022)
DOI: 10.1007/s11814-021-0972-4

pISSN: 0256-1115
eISSN: 1975-7220

Date seed activated carbon decorated with CaO and Fe_3O_4 nanoparticles as a reusable sorbent for removal of formaldehyde

Hossein Khaleghi*, Hossein Esmaeili,†, Neamatollah Jaafarzadeh*,***, and Bahman Ramavandi****,***

*Department of Environment, Bushehr Branch, Islamic Azad University, Bushehr, Iran
**Department of Chemical Engineering, Bushehr Branch, Islamic Azad University, Bushehr, Iran
***Environmental Technologies Research Center, Ahvaz Jundishapur University of Medical Sciences, Ahvaz, Iran (Invited Advisor)
****Department of Environmental Health Engineering, Faculty of Health and Nutrition, Bushehr University of Medical Sciences, Bushehr, Iran
(*Received 11 June 2021 • Revised 29 September 2021 • Accepted 1 October 2021*)

Abstract−Activated carbon (AC) was produced from date seeds by a calcination process at 700 °C for 2 h and then its surface was improved with CaO and magnetic nanoparticles. AC/CaO/Fe_3O_4 nanocomposite was then employed to remove formaldehyde ions from aqueous media. The structural characteristics of the materials were completely studied through FT-IR, XRD, SEM, EDX, Map, VSM, BET and TEM analyses. The results showed that the nanocomposite has a mesoporous structure (average pore diameter~13 nm) with great sorption capability. Also, the utmost removal efficiency of formaldehyde using AC, AC/Fe_3O_4, CaO/Fe_3O_4 and AC/Fe_3O_4/CaO nanocomposite was 94.73, 95.67, 95.14 and 98.22%, respectively, indicating that the removal efficiency increases by improving the surface properties of the AC. Moreover, the uptake of formaldehyde using AC/Fe_3O_4/CaO nanocomposite follows the Freundlich isotherm and pseudo-2nd-order kinetic models. Furthermore, the highest sorption capacity of AC, AC/Fe_3O_4, CaO/Fe_3O_4 and AC/Fe_3O_4/CaO nanocomposite using the Langmuir model was obtained 19.86, 24.21, 21.28 and 24.01 mg/g, respectively. The thermodynamic study showed that formaldehyde sorption using all four adsorbents is exothermic and spontaneous. The reusability of the adsorbents was also evaluated after ten reuse cycles and the outcomes indicated that these four adsorbents have significant reusability. Moreover, the impact of interfering ions (e.g., carbonate, sulfate, phosphate, nitrate and chloride) showed that all of these compounds, except nitrate, had little competition with formaldehyde ions for adsorption on the nanocomposite surface.

Keywords: Date Seed Activated Carbon, Formaldehyde, Magnetic Nanoparticles, Wastewater Treatment

INTRODUCTION

Formaldehyde (CH_2O) is the most toxic chemical among the 45 organic chemicals in industrial wastewater, with harmful effects on the environment and humans [1]. It is a small chemical with high solubility, which is produced as gas or water-soluble in different industries [2,3]. Various industries, such as the production of synthetic resins, the chemical and petrochemical industries, textile, aquatics industry, producing adhesives, disinfectants and preservatives, paper, and wood manufacture use water-soluble formaldehyde containing almost 37% formaldehyde [4]. However, the maximum allowable amount of formaldehyde in water sources should be 1 mg/L. Therefore, the removal of formaldehyde from the aquatic solutions is one of the major challenges in the field of industrial wastewater treatment [5].

Electronic supplementary material The online version of this article (https://doi.org/10.1007/s11814-021-0972-4) contains supplementary material, which is available to authorized users.

†To whom correspondence should be addressed.
E-mail: H.esmaeili@iaubushehr.ac.ir, esmaeili.hossein@gmail.com

Considering the physical and chemical nature of each contaminant, there are various methods for its removal, including physical, chemical, thermal and biological methods [6-8]. Among these, biological process [9] and catalytic process [10,11] can be mentioned for the removal of formaldehyde in the gas form, and membrane filtration [12], solar thermal electrochemical process [13] and photocatalyst degradation using various nanoparticles [14,15]. A combination of ultraviolet ray and ferrate(VI) method [16] can be used to eliminate formaldehyde in the form of gas and liquid. Many of these technologies have high costs for design and implementation, but the uptake method, with low costs for design and implementation, is considered as one of the cheaper methods [17-19]. According to reports, the uptake procedure is cheaper, more efficient, and much easier to implement than other methods. Also, if the adsorbent is recyclable and inexpensive, costs will be remarkably decreased [6]. Carbon produced from human hair and sheep wool [20] and activated carbon (AC) extracted from charcoal [21] are low-cost and efficient sorbents to separate formaldehyde. Other sorbents employed to eliminate formaldehyde include mesosphere MIF zeolite [22], modified and natural zeolite [4], kaolin and bentonite [23], zeolites [24], and activated carbon, zeolites, mesoporous silica, and metal organic framework [25].

AC is the most abundant material in the literature utilized to sepa-

rate pollutants from wastewater. Several materials can be applied to improve the surface features of AC. Iron oxide is one of the most critical materials for improving the AC surface [26,27]. CaO also has many benefits, like low-cost, simple synthesis, high surface area and significant capacity for separating contaminants [28].

In this study, formaldehyde was separated from aquatic solutions through AC, AC/Fe_3O_4, CaO/Fe_3O_4 and AC/Fe_3O_4/CaO nano-composite. To this end, AC was produced from date seed and then modified with Fe_3O_4 and CaO. To specify the structural features of the given adsorbents, different analyses like SEM, EDAX, Map, FT-IR, XRD, and TEM were employed. Also, equilibrium, kinetic and thermodynamic behavior of the sorption process was completely studied. To the best of the authors' knowledge, there is no published work regarding the formaldehyde removal by these adsorbents. Also, a comparison was performed between these adsorbents to remove formaldehyde. Moreover, the impact of interfering ions on the formaldehyde removal using these adsorbents was investigated.

EXPERIMENTAL SECTION

1. Materials

Sodium hydroxide (NaOH), formaldehyde (COH_2), iron (III) chloride ($FeCl_3$), iron (II) chloride ($FeCl_2$) and calcium carbonate ($CaCO_3$) were purchased from Merck (Germany). NaOH and HCl (1 molar) were used to regulate pH.

2. Synthesis of the Composite

The adsorbents used in this study are activated carbon prepared from date seeds, AC/Fe_3O_4 composite, and AC/Fe_3O_4/CaO composite, which were synthesized using chemical coprecipitation (Fig. 1). To generate the activated carbon from date seeds, the seeds were washed several times by water and completely cleaned by a knife. The cleaned seeds were put in a furnace at 400 °C for 2 h to dry, then taken out and turned into powder. For activation, the resulting powder was put into the sodium hydroxide solution. Then, the activated carbon was separated from the solution and put in the furnace at 700 °C for 2 h. Next, the activated carbon powder was placed at room temperature to cool completely and washed with distilled water several times until its pH reached 7 and was neutralized [29,30]. To synthesize the AC/Fe_3O_4 nano-composite, a solution containing Fe^{2+} and Fe^{3+} with a molar ratio of 1 and 2 was prepared and then 2 g of the activated carbon was added to the ferrous solution and mixed by a magnet-stirrer. After 50 min, NaOH solution was added to it dropwise and the magnetic composite was separated from the solution using a magnet and washed several times to neutralize its pH. It was placed in the oven to dry. To put calcium oxide on the surface of the nano-composite, first, 2 g of calcium carbonate ($CaCO_3$) was added to water. Calcium carbonate is insoluble in water and the resulting solution is heterogeneous. Then, 1 g of magnetic nano-composite (AC/Fe_3O_4) was added to it and the mixture were stirred using a magnetic-stirrer. The resulting magnetic nano-composite was separated from the solution using an external magnetic field and dried inside the oven. Next, it was placed in the furnace at 700 °C to convert $CaCO_3$ to CaO. Then, the resulting nano-composite was turned into powder using a mill and applied as an adsorbent to adsorb formaldehyde.

3. Adsorption Experiment

The experiments of formaldehyde adsorption using AC, AC/Fe_3O_4 and AC/Fe_3O_4/CaO composite were discontinuously, in stages, performed in the Erlenmeyer with a volume of 250 mL containing 100 mL of formaldehyde solution and the mixing rate of 500 rpm. To examine the impact of initial pH on the elimination efficiency of formaldehyde, the initial pH of the suspensions was set at the range of 2-10. Then, 0.2 g of adsorbent (2 g/L) was added to 100 mL of solution containing 1 mg of formaldehyde and mixed by the magnetic stirrer at 25 °C for 100 min. The samples were filtered and the solid phase (adsorbents) was separated from the liquid phase and the remaining amount of formaldehyde in solutions was measured by the spectrophotometer UV-vis (Varian, Cary 100) in the wavelength range of the ultraviolet light. The impact of

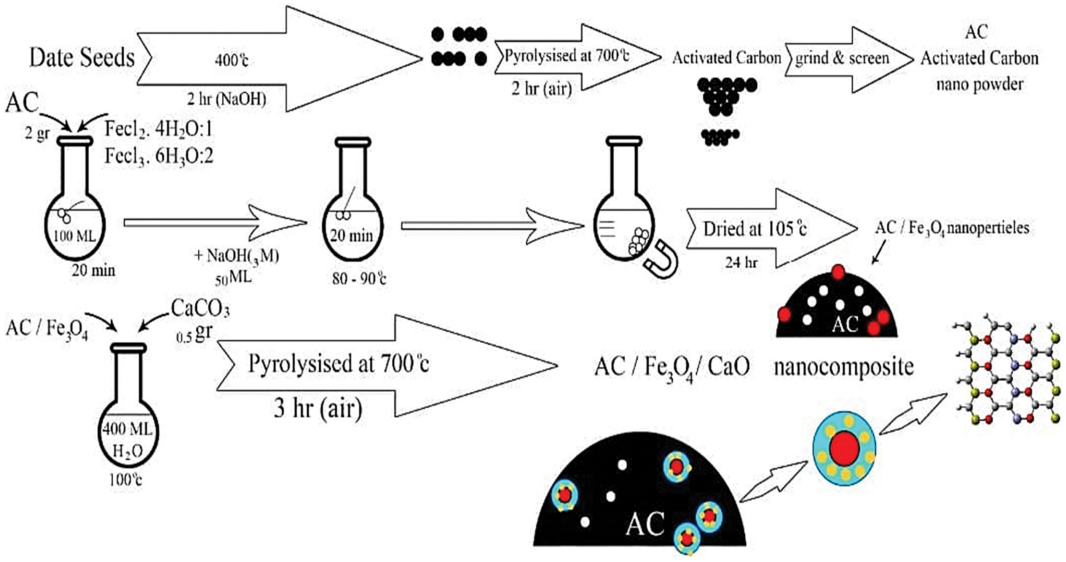

Fig. 1. Schematic of the adsorbent synthesis.

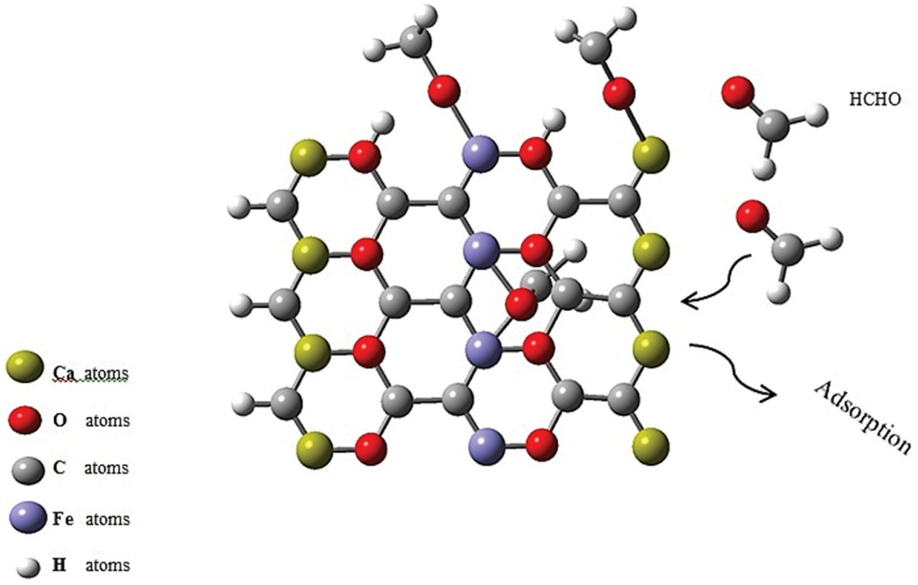

Fig. 2. Proposed mechanism of formaldehyde removal using the AC/Fe_3O_4/CaO nanocomposite.

other factors like contact time (5-150 min), sorbent dosage (0.25-5 g/L), initial formaldehyde concentration (5-50 mg/L), and temperature (25-50 °C) on the removal efficiency of formaldehyde was investigated. After the final concentration of formaldehyde was determined, the uptake efficiency (R) and uptake capacity (q_e, mg/g) were calculated as follows:

$$R(\%) = \frac{C_i - C_o}{C_o} \times 100 \quad (1)$$

$$q_e = \frac{C_i - C_o}{W} \times V \quad (2)$$

where, C_i and C_e are the initial and final concentration of formaldehyde in the aquatic solution (mg/L), W is the mass of the adsorbent (g), and V is the solution volume (L).

A proposed mechanism of the uptake process on the nanocomposite surface is illustrated in Fig. 2. As illustrated, the formaldehyde molecule attaches to the active sites on the nanocomposite surface and this pollutant can be eliminated from the suspension. The adsorption and desorption of formaldehyde involves two steps: 1) penetration of formaldehyde into the pores inside the AC/Fe_3O_4/CaO nanocomposite; 2) adsorption of formaldehyde onto the AC/Fe_3O_4/CaO nanocomposite with the help of functional groups on its surface. To this end, weak chemical interaction occurs between oxygen and carbon atoms in the formaldehyde molecule and the Fe atom on the adsorbent surface. However, the interaction between the O atom in formaldehyde and the F atom at the Fe_3O_4 surface is predominant. Also, formaldehyde prefers to absorb on the Fe atom to the O atom and pore sites [31]. Ca-O bond plays an important role in the adsorption of formaldehyde. To do so, the oxygen atom in formaldehyde may bind to the Ca-O bond [32]. Moreover, formaldehyde can be chemically adsorbed using the C atom in activated carbon [33]. Therefore, Fe, C atoms and Ca-O bond are effective elements in the AC/Fe_3O_4/CaO nanocomposite for the removal of formaldehyde from aqueous solution.

4. Equilibrium Study of the Uptake Process

Adsorption isotherms give critical information about the distribution of contaminants (adsorbates) within the adsorbent pores [34,35]. In this research, the equilibrium study of the uptake process was investigated using known isotherm models such as Langmuir, Freundlich and Dubinin-Radushkevich (D-R). The uptake process of formaldehyde was studied using the AC, AC/Fe_3O_4 and AC/Fe_3O_4/CaO nanocomposite in different formaldehyde concentrations. The nonlinear form of the Langmuir, Freundlich and D-R models is presented in Eqs. (3) to (5), respectively [36,37].

$$q_e = \frac{q_m k_L C_e}{1 + k_L C_e} \quad (3)$$

$$q_e = k_f C_e^{1/n} \quad (4)$$

$$q_e = q_m \exp(-\beta(RT\ \mathrm{Ln}(1 + (1/C_e)))^2) \quad (5)$$

where, q_e, C_e, q_m, k_L, k_f, n and β are the amount of formaldehyde adsorbed per gram of the adsorbent (mg/g), the formaldehyde concentration in the solution at equilibrium time (mg/L), the uptake capacity (mg/g), the sorption energy, the Freundlich constant, the Freundlich constant depending on the sorption intensity, and the Dubinin-Radushkevich constant depending on the sorption energy, respectively. To calculate the parameters of the Langmuir, Freundlich and D-R models, q_e and C_e were determined for each experiment and then the plot of q_e against C_e was drawn. Equilibrium isotherms for the sorption of formaldehyde onto AC, AC/Fe_3O_4 and AC/Fe_3O_4/CaO nanocomposite were experimentally obtained for different formaldehyde concentrations (5-50 mg/L). The Langmuir, Freundlich and D-R parameters were calculated using nonlinear regression analysis of the corresponding models. Microsoft Excel solver and "trial and error" method were employed to calculate the parameters of equilibrium isotherms and minimize the error values [37].

The main characteristic of the Langmuir model can be calculated using a dimensionless constant (R_L):

$$R_L = \frac{1}{1+K_L C_i} \quad (6)$$

where K_L and C_i are the Langmuir constant and initial concentration of formaldehyde, respectively. If $R_L>1$, $R_L=1$, $0<R_L<1$ and $R_L=0$, the sorption process is defined as unfavorable, linear, favorable, and irreversible, respectively [36].

Also, in the D-R model, the average sorption energy (E) gives critical information about the sorption mechanism and is defined to transfer 1 mole of the pollutant to the sorbent surface, which is calculated as follows:

$$E = \frac{1}{\sqrt{2\beta}} \quad (7)$$

If E<8 KJ/mol and 8 KJ/mol<E<16 KJ/mol, the sorption process will be physical and chemical, respectively [36].

5. Kinetic Study

Kinetic parameters give important information for designing and modeling the uptake processes. In this study, kinetic models were used to examine the kinetic behavior of formaldehyde sorption using the AC, AC/Fe_3O_4 and AC/Fe_3O_4/CaO nanocomposite. Formaldehyde adsorption kinetics using the aforementioned adsorbents is necessary to choose the best operational conditions for the sorption process in industrial applications. Therefore, the formaldehyde sorption kinetics was examined using common kinetic models such as pseudo-1st-order (Eq. (8)) and pseudo-2nd-order (Eq. (9)) as follows [38].

$$q_t = q_e(1-e^{-k_1 t}) \quad (8)$$

$$q_t = \frac{k_2 q_e^2 t}{1+k_2 q_e t} \quad (9)$$

In these Eqs., q_t and q_e are the sorption capacity at time t and equilibrium time (mg/g), respectively. Also, t, k_1 and k_2 are contact time (min), the pseudo-1st-order kinetic constant and the pseudo-2nd-order kinetic constant, respectively. Microsoft Excel solver and "trial and error" were employed to calculate the parameters of kinetic models and minimize the error values (Similar to isotherm models).

6. Thermodynamic Study

Thermodynamic study of the uptake process is necessary to determine whether the sorption process is spontaneous or not. Gibbs free energy indicates the spontaneity of a chemical reaction [39]. To this end, enthalpy changes (ΔH^o), Gibbs free energy changes (ΔG^o), and entropy changes (ΔS^o) were calculated to have a better understanding of the sorption mechanism. The relationship between these parameters is defined as follows [40]:

$$\ln(1{,}000 \times k_c) = \frac{\Delta S^o}{R} - \frac{\Delta H^o}{R}\left(\frac{1}{T}\right) \quad (10)$$

$$\Delta G^o = -RT\ln(1{,}000 \times k_c) \quad (11)$$

$$k_c = \frac{q_e}{C_e} \quad (12)$$

where k_c, R and T are the distribution constant, the universal gas constant (8.314 J/mol·K), and the absolute temperature (K), respectively [36].

7. Characterization of the Adsorbents

Various analyses were performed to investigate the sorbent properties. FTIR analysis was done using a Bruker Vector 22 machine to specify functional groups in the adsorbents surface. To examine the surface changes of the adsorbents as well as the elemental compositions in the adsorbents structure, SEM, EDX and Map (SEM-TESCAN MIRA3-FEG) analyses were employed. XRD analysis (Philips PW 1730) was used to specify crystalline structure of the AC, CaO, AC/Fe_3O_4 and AC/Fe_3O_4/CaO. TEM analysis (Leo 906 model at the voltage of 80 KV) was used to evaluate the shape and size of the particles in the structure of the AC, AC/Fe_3O_4 and AC/Fe_3O_4/CaO nanocomposite. VSM analysis was employed to examine the magnetic characteristics of Fe_3O_4, AC/Fe_3O_4 and AC/Fe_3O_4/CaO composite. Furthermore, specific surface area and pore volume are among the critical features of the adsorbents and the sorption capacity depends on them. The specific surface area and pore volume of Fe_3O_4, AC/Fe_3O_4 and AC/Fe_3O_4/CaO were measured using BET analysis.

8. Desorption Experiments and the Effect of Interfering Ions

To study the desorption process, 1, 2 and 2.5 g/L of AC, AC/Fe_3O_4 and AC/Fe_3O_4/CaO nanocomposite were in turn added to the aqueous solution with the initial concentration of 5 mg/L. Then, the solutions containing AC, AC/Fe_3O_4, and AC/Fe_3O_4/CaO nanocomposite then stirred using the magnetic stirrer for 120, 100, and 100 min, respectively (each adsorbent was separately examined). After the due time was finished and the sorption process was done, the above-mentioned adsorbents were separated from the aqueous solution and then added to 30 ml of H_2SO_4 solution at concentrations of 0, 3 and 5 M and mixed with a magnetic stirrer for 150 min. The solution was filtered and the concentration of the formaldehyde separated from the adsorbents was measured. The desorption test was done up to ten steps and the desorption capability and reusability of the aforementioned adsorbents in the formaldehyde adsorption were investigated. The desorption percentage was calculated through Eq. (13).

$$\text{Desorption (\%)} = \left(\frac{\text{amount of formaldheyde desorbed}}{\text{amount of formaldheyde adsorbed}}\right) \times 100 \quad (13)$$

The impact of interfering ions such as calcium carbonate, calcium sulfate, calcium phosphate, calcium nitrate, and calcium chloride at a concentration of 3 molar on the sorption of formaldehyde was also studied. To investigate the impact of various anions on the sorption efficiency of formaldehyde, the sorption process was done under the optimized condition. Then, the residual concentration of formaldehyde in aqueous solution was measured.

RESULTS AND DISCUSSION

1. Characteristics of the Adsorbents

FT-IR analysis was applied to specify the functional groups in the structure of the AC, AC/Fe_3O_4, and AC/Fe_3O_4/CaO nanocomposite, and the outcomes are demonstrated in Fig. 3(a). As can be seen, in the structure of the AC, sorption peaks were observed at

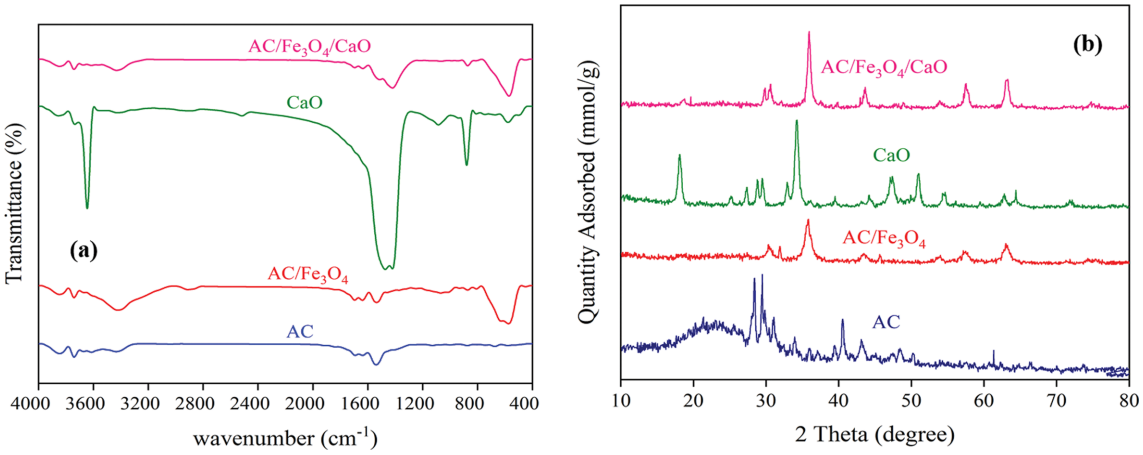

Fig. 3. The results of FT-IR (a) and XRD (b) analyses.

3,740, 3,614, and 3,434 cm^{-1}, which are attributed to the O-H and hydrogen bonds in its structure. Also, some other sorption peaks were observed at 1,539, 1,637, and 1,692 cm^{-1}, which are related to C=C bonds of alkene and aromatic [41]. In the AC/Fe_3O_4 structure, the sorption peaks in the AC structure such as 3,740, 3,614, and 3,434 cm^{-1} were shifted to 3,847, 3,741, and 3,422 cm^{-1}, respectively. The peaks at 1,539, 1,637 and 1,692 cm^{-1} were transferred to 1,535, 1,638, and 1,695 cm^{-1}, respectively. A strong sorption peak appeared at 574 cm^{-1}, which is attributed to the Fe-O vibrations and confirms that Fe_3O_4 nanoparticles are present in the structure of the given composites [42]. A strong adsorption peak was seen at 3,645 cm^{-1} in the structure of CaO, which can be due to the OH bond of the hydroxyl groups (Ca-OH). Widespread adsorption peaks were observed at 1,420 and 1,472 cm^{-1}, which indicate the presence of mono and pair carbonates in the CaO structure [43]. Another sorption peak was observed in the CaO structure at 876 cm^{-1}, which is attributed to the C-H bending aromatic bonds [44]. After synthesis of AC/Fe_3O_4/CaO nanocomposite, the sorption peaks in the CaO structure were observed with slight changes in intensity in the AC/Fe_3O_4/CaO structure. For example, two peaks at 574 and 876 cm^{-1} were shifted to 570 and 871 cm^{-1}, respectively, and peaks of 1,420 and 1,472 cm^{-1} were shifted to 1,419 and 1,513 cm^{-1}. Furthermore, two peaks at 3,400 and 3,800 cm^{-1} were observed in the AC/Fe_3O_4/CaO structure, indicating that the AC/Fe_3O_4/CaO nanocomposite is well synthesized and there are Fe_3O_4 and calcium oxide in the activated carbon structure.

XRD analysis was done to examine the crystal structure of the AC, AC/Fe_3O_4 and AC/Fe_3O_4/CaO in the range of 5 to 80° and the outcomes are illustrated in Fig. 3(b). Regarding the findings, some peaks with different intensities appeared in the structure of AC, AC/Fe_3O_4 and AC/Fe_3O_4/CaO, which shows crystalline and semi-crystalline phases in the structure of the mentioned materials. Therefore, it is concluded that the structure of all the mentioned materials is crystalline. In the AC structure, some peaks were observed at 2θ of 20.29 and 43.61°, which are attributed to the crystalline phases of (002) and (001) and are related to the structure of the graphite [45,46]. Other peaks were observed at 29.39, 36.04, 40.54, and 64.84, which are related to the crystalline phases of (220), (311), (222), and (440), respectively [47,48]. In the structure of AC/Fe_3O_4 nanocomposite, several peaks were observed at 30.34, 35.84, 43.29, 53.79, 57.14 and 63.24°, which are attributed to the crystalline phases of (220), (311), (400), (422), (511) and (440), respectively, indicating that Fe_3O_4 nanoparticles formed in the AC are of reverse cubic spinel-type [49-51]. Furthermore, concerning the XRD analysis for CaO, several peaks were observed at 2θ of 17.99, 33.94, 34.29, 39.94 and 54.36°, which had been observed in the structure of calcium oxide in the previous studies as well. Also, in the structure of the AC/Fe_3O_4/CaO nanocomposite, some peaks were observed at 2θ of 18.79, 29.74, 34.29, 35.94, 43.49, 53.99, 57.54 and 63.29°, which indicate the presence of CaO in the structure of the AC/Fe_3O_4 composite and formation of the AC/Fe_3O_4/CaO nanocomposite [42,52].

Surface morphology and features, elemental compounds, and their percentage in the structure of AC, CaO, AC/Fe_3O_4 and AC/Fe_3O_4/CaO composites were examined using SEM, EDX and Map analyses, and the results are illustrated in Figs. 4 and 5. The percentage of elements in the structure of materials is given in Table 1. As can be seen, the activated carbon produced from date seed has a flat and porous surface (Fig. 4(c)-(d)). After placement of Fe_3O_4 nanoparticles on the AC surface, some particles in different sizes are observed that can result from the formation of Fe_3O_4 nanoparticles on the surface of the AC, leading to surface changes and unevenness (Fig. 4(d)). SEM analysis for CaO (Fig. 4(a)) shows that there are many pores on its structure [48]. Moreover, surface morphology of the AC/Fe_3O_4/CaO nanocomposite has surface unevenness, high porousness and layered structures that can be effective in the uptake process of various contaminants (Fig. 4(g)). The results of EDX and Map analyses also confirm the placement of Fe_3O_4 nanoparticles and CaO on the AC surface. Elements of carbon (74.58%) and oxygen (25.42%) were observed in the AC structure. After the AC/Fe_3O_4/CaO nanocomposite was prepared, the distribution of elements in the AC/Fe_3O_4/CaO nanocomposite structure included carbon (22.53%), oxygen (29.62%), calcium (5.67%) and Fe (42.19%), which demonstrate a proper distribution of the elements.

In addition to SEM analysis, TEM analysis was also used to investigate the morphology and structure of the date seed-derived AC, CaO, AC/Fe_3O_4 and AC/Fe_3O_4/CaO nanocomposite (Fig. 6).

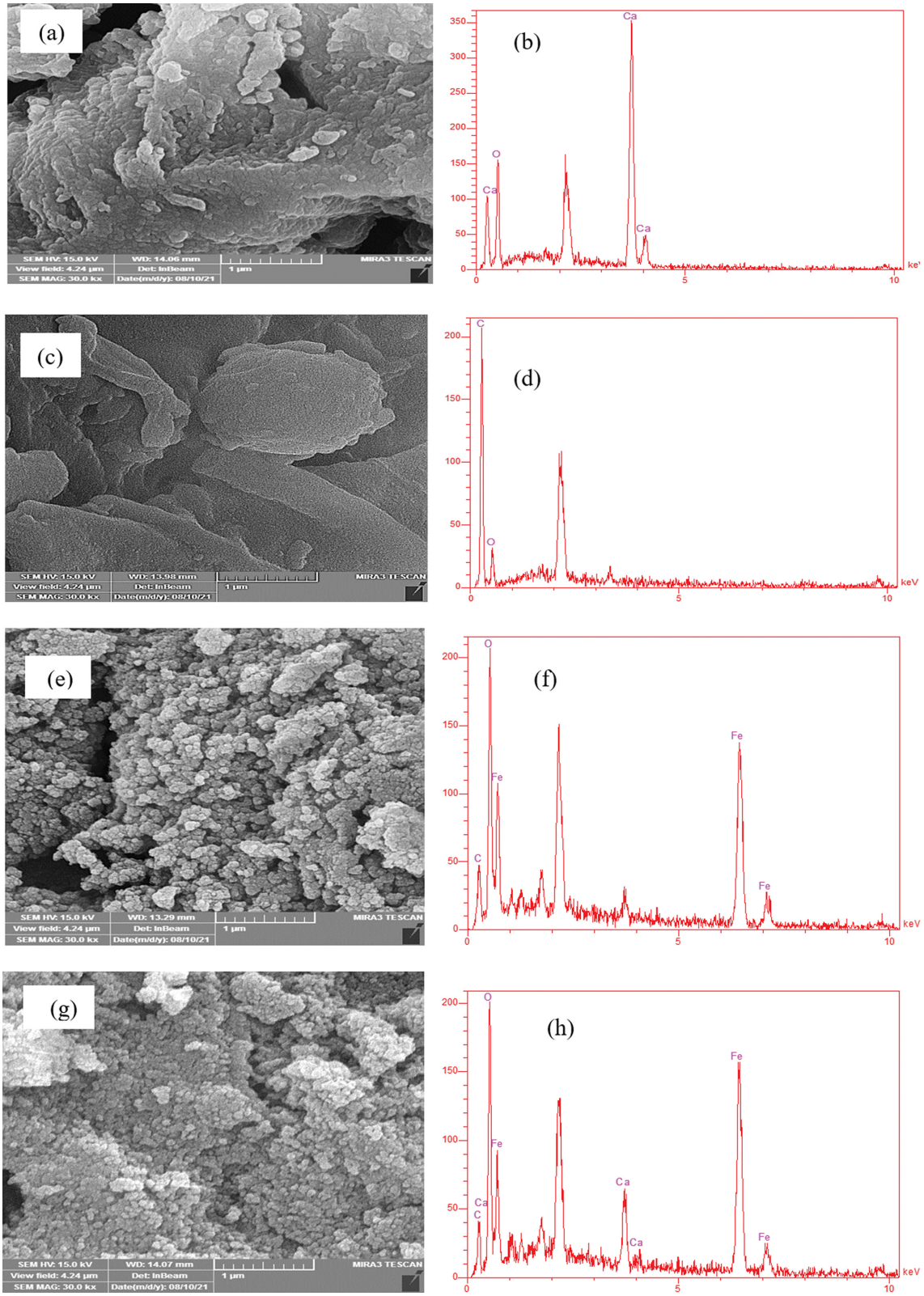

Fig. 4. The results of SEM and EDX analyses for CaO ((a) and (b)), AC ((c) and (d)), AC/Fe_3O_4 composite ((e) and (f)), and AC/Fe_3O_4/CaO ((g) and (h)).

The findings indicate that AC and CaO have a very good, layered surface, which is also proved in the results of SEM analysis (Fig. 4). As shown in Fig. 6(d), the morphology of the AC/Fe_3O_4 composite confirms that Fe_3O_4 nanoparticles with a spherical structure are

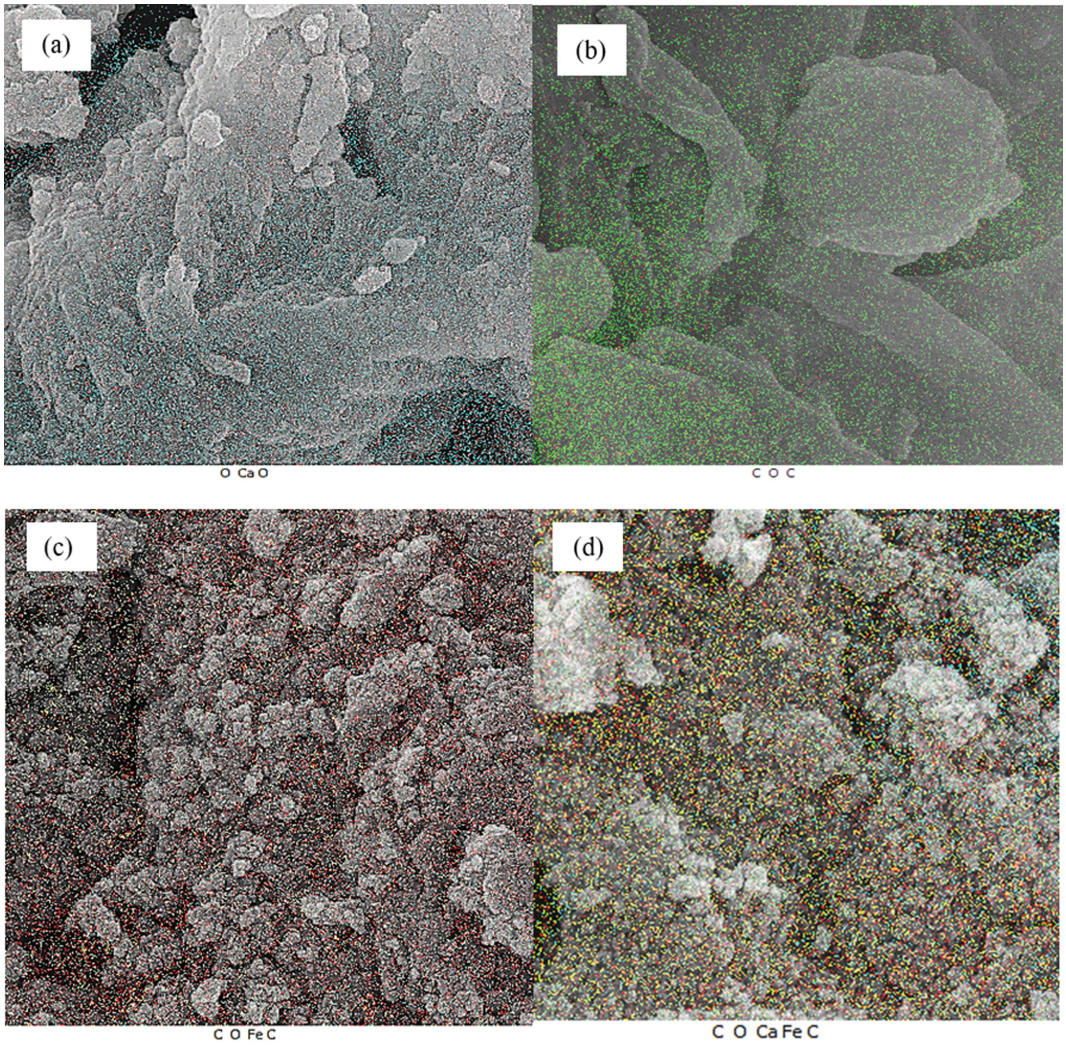

Fig. 5. Mapping analysis for (a) CaO (O: red dots and Ca: blue dots), (b) AC (O: red dots and C: green dots), (c) AC/Fe_3O_4 composite (O: red dots, C: blue dots and Fe: green dots) and (d) AC/Fe_3O_4/CaO (O: red dots, Ca: blue dots, C: yellow dots and Fe: green dots).

Table 1. Distribution of elements in CaO, AC, AC/Fe_3O_4 and AC/CaO/Fe_3O_4

Element	CaO wt%	AC wt%	AC/Fe_3O_4 wt%	AC/CaO/Fe_3O_4 wt%
Ca	43.41	-	-	5.67
O	56.59	25.42	37.01	29.62
C	-	74.58	30.04	22.53
Fe	-	-	32.95	42.19
Total	100	100	100	100

successfully distributed on the AC surface and have a suitable interaction [28]. After the formation of the AC/Fe_3O_4/CaO nanocomposite, the outcomes showed that there are Fe_3O_4 nanoparticles, AC and CaO in the composite structure (Fig. 6(d)) and is compatible with the findings of SEM, analysis.

The magnetic characteristics of Fe_3O_4 nanoparticles, AC/Fe_3O_4 and AC/Fe_3O_4/CaO nanocomposite were investigated using VSM analysis and the outcomes are illustrated in Fig. 7. As can be seen, Fe_3O_4 nanoparticles have higher magnetic saturation (80.63 emu/g) than AC/Fe_3O_4 composite (43.84 emu/g) and AC/Fe_3O_4/CaO nanocomposite (28.75 emu/g), which can be due to various factors such as the size of particles, the existence of oxygen on the particles [53] and non-magnetic materials such as activated carbon and calcium oxide in the structure of AC/Fe_3O_4 and AC/Fe_3O_4/CaO composites [49]. Also, the charts are s-shaped for all the four materials, which signifies the paramagnetic feature of the mentioned materials and confirms that they can be easily separated from the aquatic solutions through an external magnetic field.

The results of BET analysis for the AC, CaO, AC/Fe_3O_4 and AC/Fe_3O_4/CaO nanocomposite are reported in Table 2. The specific surface area for the AC, CaO, AC/Fe_3O_4 and AC/Fe_3O_4/CaO was obtained 413.05, 2.459, 89.964, and 59.192 m^2/g, respectively. The specific surface area of AC was significantly higher than that of other adsorbents, and this value was the lowest for CaO. The mean pore volume for the AC, CaO, AC/Fe_3O_4, and AC/Fe_3O_4/CaO was determined as 0.2, 0.017, 0.211, and 0.193 cm^3/g, respec-

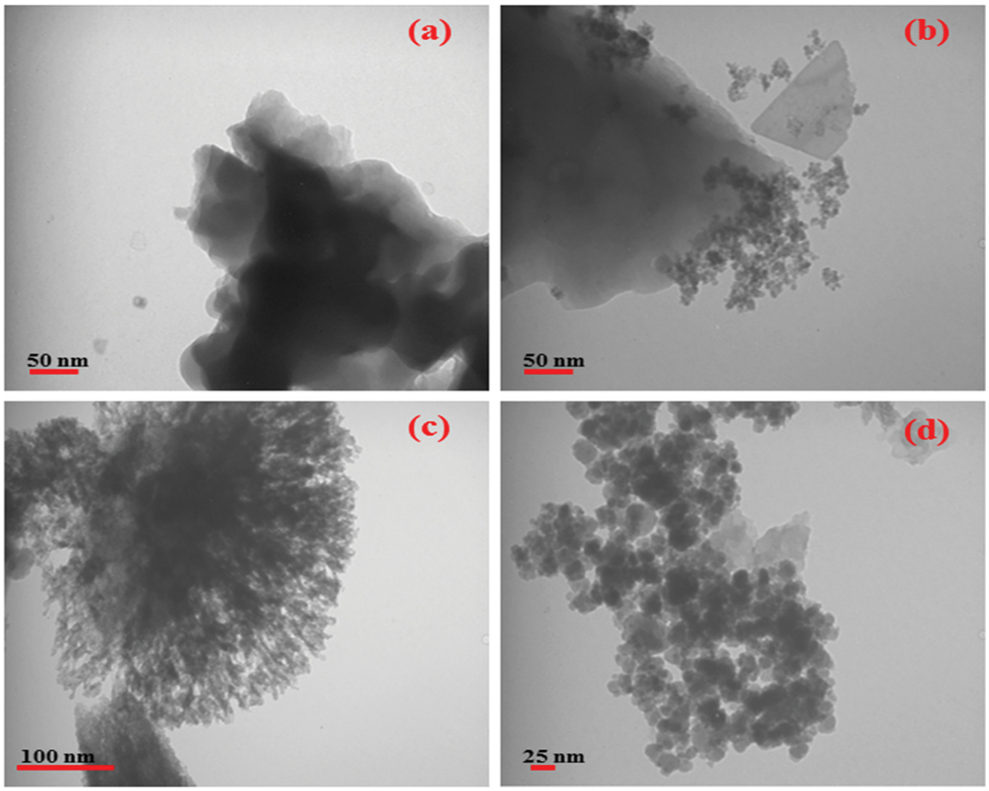

Fig. 6. The results of TEM analysis for (a) AC (b) AC/Fe_3O_4 composite (c) CaO (d) AC/Fe_3O_4/CaO nanocomposite.

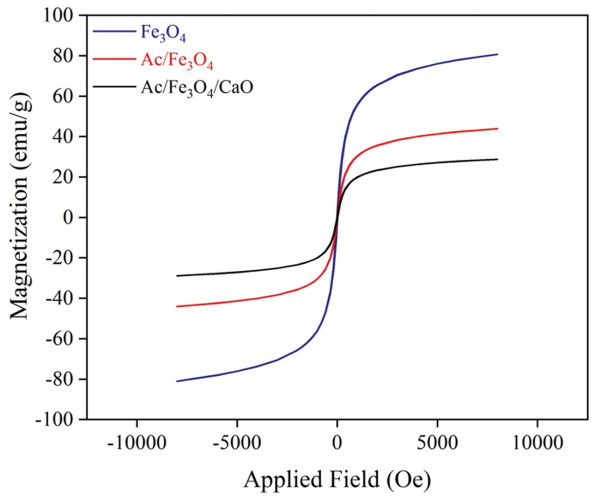

Fig. 7. VSM analysis for Fe_3O_4, AC/Fe_3O_4 and AC/Fe_3O_4/CaO nanocomposite.

tively. The specific surface area and pores volume are critical parameters in the sorption process because they have a direct impact on the sorption capacity of contaminants. As can be seen, these amounts are appropriate for AC, AC/Fe_3O_4 and AC/Fe_3O_4/CaO adsorbents, which indicates the high uptake capacity of these sorbents.

2. Impact of Various Factors on the Uptake Process

Initial pH is one of the most important and effective factors in the uptake of various contaminants [48]. Therefore, its impact on the elimination efficiency of formaldehyde using AC, AC/Fe_3O_4, CaO/Fe_3O_4 and AC/Fe_3O_4/CaO nanocomposite was investigated and the outcomes are illustrated in Fig. 8(a). As can be seen, as pH increases from 2 to 7, the sorption efficiency of formaldehyde using all the four adsorbents increases and then decreases from 7 to 11. Therefore, the best pH for the formaldehyde uptake using the mentioned sorbents was 7. At pH<7, hydrogen ions (H^+) in the solution compete with formaldehyde ions, which leads to a decrease in the removal efficiency of formaldehyde [54]. Also, the removal percentage was decreased at pH>7, which is due to the competi-

Table 2. Surface characteristics of AC, CaO, AC/Fe_3O_4 and AC/Fe_3O_4/CaO

Parameter	AC	CaO	AC/Fe_3O_4	AC/Fe_3O_4/CaO
BET surface area (m^2/g)	413.05	2.459	89.964	59.192
Langmuir surface area (m^2/g)	545.22	2.798	82.098	59.917
Total pore volume (cm^3/g)	0.2	0.017	0.211	0.193
Adsorption mean pore diameter (°A)	19.46	27.69	9.388	13.02
BJH Adsorption mean pore diameter (°A)	37.1	7.99	4.03	2.38

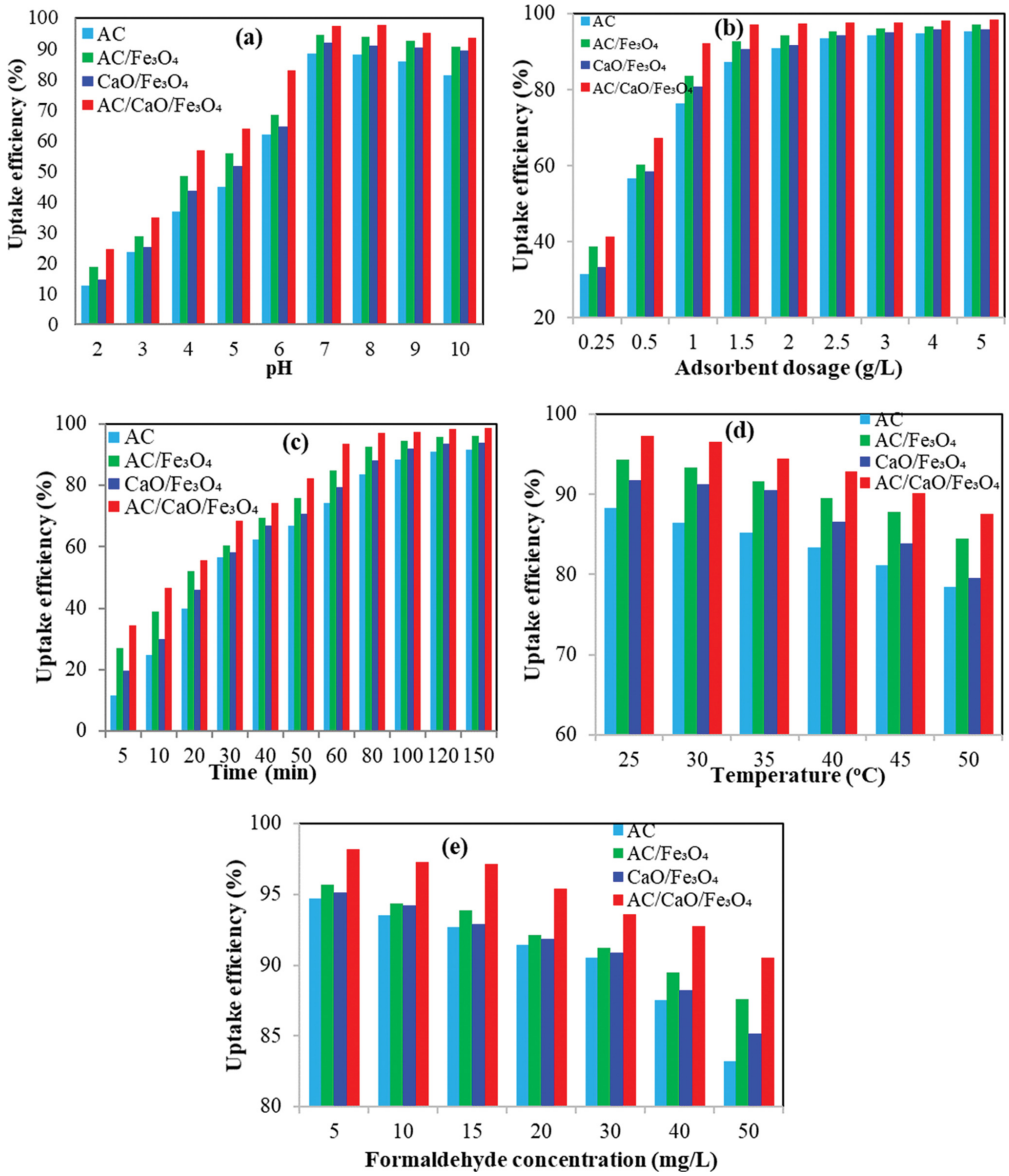

Fig. 8. The impact of initial pH (a), adsorbent dosage (b), time (c), temperature (d), and formaldehyde concentration (e) on the uptake efficiency of formaldehyde through AC, AC/Fe_3O_4, CaO/Fe_3O_4 and AC/Fe_3O_4/CaO nanocomposite.

tion of hydroxide ions (OH^-) and formaldehyde ions for adsorption on the adsorbents surface [55].

Adsorbent dosage is another critical factor in the sorption process and has an essential role in increasing its efficiency [56]. Therefore, the sorption process of formaldehyde using AC, AC/Fe_3O_4, CaO/Fe_3O_4 and AC/Fe_3O_4/CaO composite was performed at pH7, initial formaldehyde concentration of 10 mg/L, temperature of 25 °C, and contact time of 100 min. The outcomes are illustrated in Fig. 8(b). As shown, the uptake efficiency increased with increasing the sorbent dosage as well as active sites of the sorbent [23,57]. The sorption efficiency using the AC, CaO/Fe_3O_4 and AC/Fe_3O_4 increased with increasing the dose of adsorbents up to 3 g/L and after that, its value remained almost constant. According to the results, the optimal adsorbent dosage for AC, CaO/Fe_3O_4 and AC/Fe_3O_4 was determined as 3 g/L, and for the AC/Fe_3O_4/CaO nanocomposite, the optimal adsorbent dosage was 2.5 g/L.

Contact time is also an effective parameter in the uptake process and, in the present study, its effect on the formaldehyde uptake process using the AC, AC/Fe_3O_4, CaO/Fe_3O_4 and AC/Fe_3O_4/CaO nanocomposite was examined. The tests were done at pH 7, initial formaldehyde concentration of 10 mg/L, temperature of 25 °C and sorbent dosage of 3 g/L for the AC, CaO/Fe_3O_4 and AC/Fe_3O_4 nanocomposite, and 2.5 g/L for the AC/Fe_3O_4/CaO nanocomposite. The findings are illustrated in Fig. 8(c). As can be seen, the uptake efficiency of formaldehyde ion using all adsorbents increases sharply at the beginning of the sorption process (almost in the first 100 min), which is due to the large number of active sites on the adsorbent surface [23]. Then, as the contact time increases, the adsorbents are saturated by the formaldehyde molecules, and it can lead to a decrease in the slope of the uptake efficiency. As a result, the

equilibrium time was determined 100 min for the AC, CaO/Fe_3O_4 and AC/Fe_3O_4 and 80 min for the AC/Fe_3O_4/CaO nanocomposite.

Temperature is one of the most effective factors in the sorption efficiency [58]. The impact of temperature on the sorption efficiency of formaldehyde using the AC, AC/Fe_3O_4, CaO/Fe_3O_4 and AC/Fe_3O_4/CaO was studied (Fig. 8(d)). As can be seen, the uptake efficiency of formaldehyde using all the three adsorbents decreases with increasing temperature. The highest sorption efficiency was reached at ambient temperature and, consequently, for formaldehyde adsorption through these three adsorbents there is no need to heat the process. It happens at the temperature of 25 °C with the highest efficiency and it can play a very useful role in decreasing the operational costs of formaldehyde adsorption using these adsorbents.

The initial concentration of formaldehyde ion is one of the crucial factors in the adsorption process [20]. In present study, the impact of initial formaldehyde concentration on the adsorption efficiency was examined using activated carbon, AC/Fe_3O_4, and AC/Fe_3O_4/CaO nanocomposite under optimal conditions (see Fig. 8(e)). By increasing the initial formaldehyde concentration from 5 to 50 mg/L, the uptake efficiency using AC, CaO/Fe_3O_4, AC/Fe_3O_4 and AC/Fe_3O_4/CaO nanocomposite decreased from 94.73 to 83.21%, 95.14 to 85.17%, 95.67 to 87.58% and 98.22 to 90.54%, respectively. Therefore, the maximum uptake efficiency was obtained at a formaldehyde concentration of 5 mg/L. The reason for this reduction for all adsorbents can be attributed to the saturation of the active sites on the adsorbents surface at high concentrations of formaldehyde [59].

According to the achieved results in examining various factors in the uptake efficiency of formaldehyde, it is observed that AC/

Table 3. The equilibrium models and their constants

Model	Parameters	AC	AC/Fe_3O_4	CaO/Fe_3O_4	AC/Fe_3O_4/CaO
Langmuir	q_m (mg/g)	19.86	24.21	21.28	24.01
	k_L (L/mg)	0.281	0.236	0.267	0.563
	R_L	0.066-0.416	0.078-0.458	0.070-0.429	0.034-0.262
	R^2	0.998	0.995	0.998	0.977
Freundlich	n	1.842	1.613	1.749	1.921
	k_f ((mg/g)·(L/mg)$^{1/n}$)	4.596	4.801	4.628	8.192
	R^2	0.979	0.996	0.989	0.995
D-R	E (KJ/mol)	1.08	1.174	1.579	1.954
	q_m (mg/g)	12.83	13.34	13.19	15.66
	$\beta\times10^{-6}$ (mol^2/J^2)	0.427	0.363	0.419	0.131
	R^2	0.913	0.891	0.903	0.879

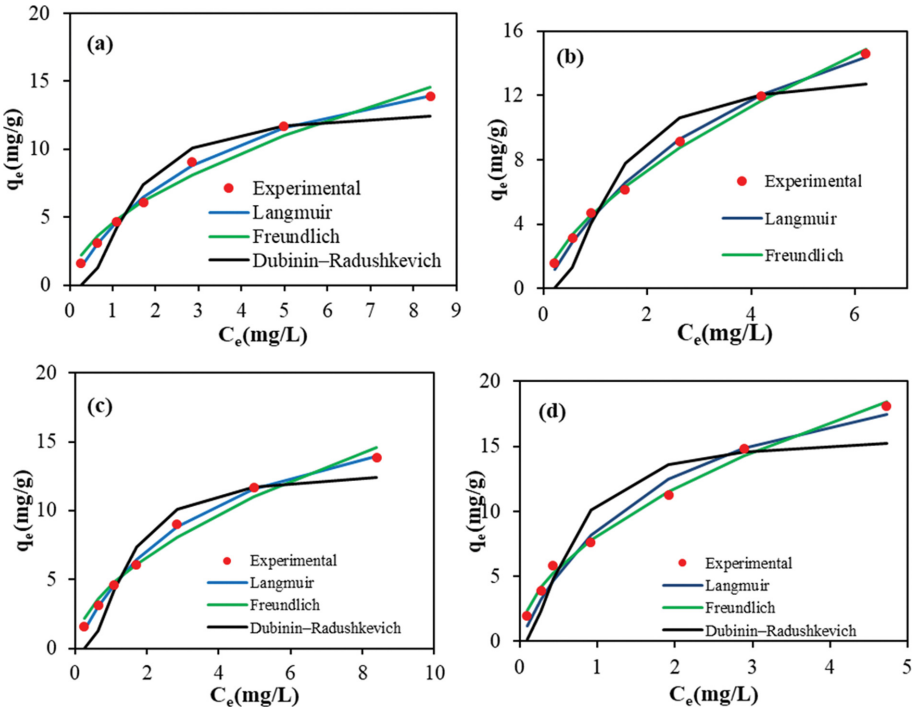

Fig. 9. Isotherm charts for AC (a), AC/Fe_3O_4 (b), CaO/Fe_3O_4 (c) and AC/Fe_3O_4/CaO (d).

Fe_3O_4/CaO composite has the highest uptake efficiency among the four adsorbents. Also, the optimal values of adsorbent dose and contact time in the adsorption process using the AC/Fe_3O_4/CaO nanocomposite were less than the other two sorbents. The lowest sorption efficiency in all experiments was obtained using AC. Therefore, surface modification of AC by Fe_3O_4 nanoparticles and CaO/Fe_3O_4 magnetizes it and makes it easy to separate from the solution. It leads to a decrease in the contact time and adsorbent dosage and also increases the uptake efficiency of formaldehyde. Therefore, the surface modification of AC increases the uptake efficiency of formaldehyde and decreases the operational costs of the uptake process. A comparison between CaO/Fe_3O_4 and AC/Fe_3O_4/CaO indicates that the addition of activated carbon to the CaO/Fe_3O_4 structure increases the uptake efficiency of formaldehyde ion from 95.14% to 98.22%.

3. Equilibrium Study

In present study, the sorption isotherm was examined under the optimized pH and the initial formaldehyde concentration in the range of 5 to 50 mg/L. The results of adsorption isotherms are presented in Table 3 and Fig. 9. The value of R_L obtained by the Langmuir model for the adsorbents was between 0-1 and the value of n obtained by the Freundlich model was higher than 1, indicating that the formaldehyde sorption process using all four adsorbents is favorable and physical [29,60]. The value of parameter E calculated by the Dubinin-Radushkevich model was less than 8, indicating that the adsorption process is physical [43]. Moreover, the maximum sorption capacity of AC, AC/Fe_3O_4, CaO/Fe_3O_4 and AC/Fe_3O_4/CaO nanocomposite using the Langmuir model was obtained 19.86, 24.21, 21.28 and 24.01 mg/g, respectively, indicating that AC/Fe_3O_4/CaO nanocomposite has a higher sorption capacity than other adsorbents. According to the correlation coefficient (R^2) obtained for all three models, the Freundlich was found to be the best model for describing the formaldehyde sorption process using the AC/Fe_3O_4 and AC/Fe_3O_4/CaO. Therefore, formaldehyde

Table 4. Kinetic models and their calculated parameters

Kinetic model	Parameters	AC	AC/Fe_3O_4	CaO/Fe_3O_4	AC/Fe_3O_4/CaO
Pseudo-1st-order	$q_{e.\,Cal}$ (mg/g)	0.310	0.316	0.314	0.387
	k_1 (1/min)	0.028	0.038	0.032	0.047
	R^2	0.996	0.955	0.988	0.916
Pseudo-2nd-order	$q_{e.\,Cal}$ (mg/g)	0.393	0.374	0.385	0.444
	k_2 (g/mg·min)	0.071	0.123	0.090	0.142
	R^2	0.994	0.98	0.994	0.959
	$q_{e.\,exp}$ (mg/g)	0.305	0.321	0.313	0.395

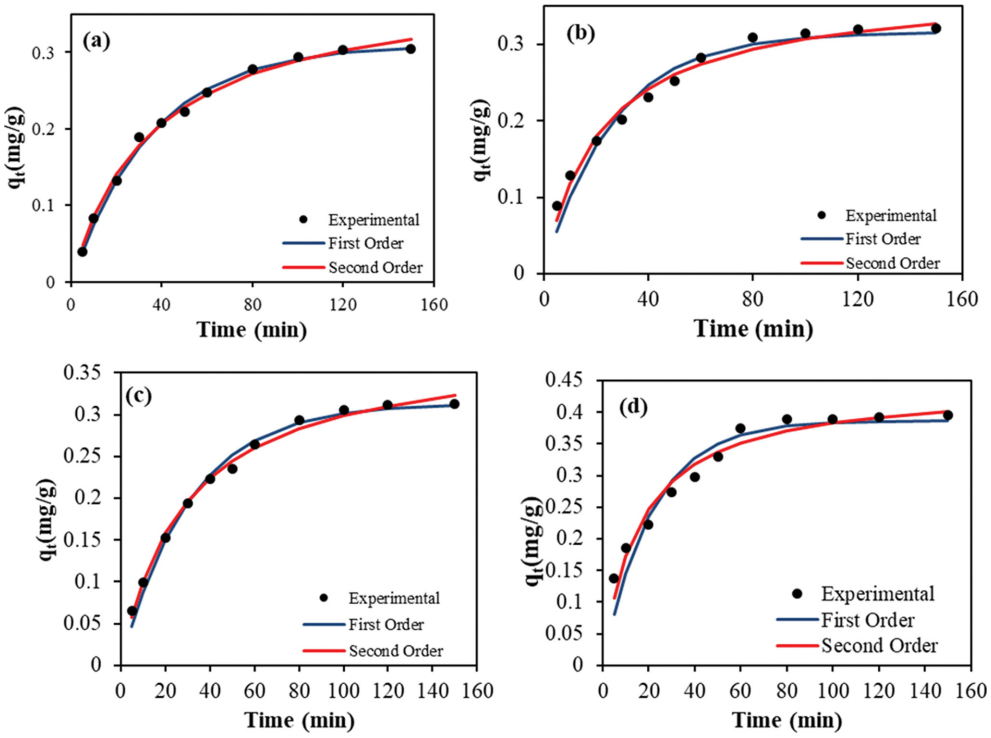

Fig. 10. The chart of non-linear kinetic models for the formaldehyde sorption from aquatic solution using AC (a), AC/ Fe_3O_4 (b), CaO/Fe_3O_4 (c) and AC/ Fe_3O_4/CaO (d).

adsorption by these adsorbents takes place on the adsorbents' heterogeneous surfaces. Also, the adsorption sites on the adsorbent's surface have different adsorption energy [38,61]. Furthermore, the findings showed that the formaldehyde sorption process using the AC and CaO/Fe_3O_4 follows the Langmuir model [60]. Thus, formaldehyde sorption takes place on the homogeneous surfaces of the AC/Fe_3O_4 composite and adsorption is monolayer.

4. Sorption Kinetics

In the present study, the pseudo-1st-order and pseudo-2nd-order kinetic models were used to investigate the rate and kinetics of the formaldehyde sorption process (Table 4 and Fig. 10). As can be seen, the best model to express the kinetics of the formaldehyde sorption process using the AC/Fe_3O_4, CaO/Fe_3O_4 and AC/Fe_3O_4/CaO composites was the pseudo-2nd-order kinetic model. Also, the value of the adsorption capacity obtained at the equilibrium time utilizing the pseudo-2nd-order kinetic model is closer to the experimental data, which confirms the suitability of the pseudo-2nd-order model [42]. The value of R^2 for the pseudo-1st-order kinetic model in adsorption of formaldehyde using the AC was higher than that of pseudo-2nd-order model, and the uptake capacity calculated from that was closer to the experimental data. Therefore, the formaldehyde uptake process using the AC follows the pseudo-1st-order kinetic model.

Table 5. The thermodynamic parameters of the formaldehyde uptake process using the AC, AC/Fe_3O_4, CaO/Fe_3O_4 and AC/Fe_3O_4/CaO nanocomposite

Adsorbent	T (°C)	ΔG^o (KJ/mol)	ΔH^o (KJ/mol)	ΔS^o (J/mol·K)
AC	25	−7.413	−51.52	−22.79
	30	−7.109		
	35	−6.969		
	40	−6.726		
	45	−6.415		
	50	−6.068		
AC/Fe_3O_4	25	−9.391	−88.76	−35.93
	30	−9.093		
	35	−8.623		
	40	−8.106		
	45	−7.785		
	50	−7.164		
CaO/Fe_3O_4	25	−7.368	−35.28	−92.52
	30	−7.319		
	35	−7.227		
	40	−6.331		
	45	−5.838		
	50	−5.156		
AC/Fe_3O_4/CaO	25	−10.87	−145.24	−54.21
	30	−10.354		
	35	−9.273		
	40	−8.723		
	45	−7.942		
	50	−7.350		

5. Thermodynamic Study

Different thermodynamic parameters such as enthalpy changes (ΔH^o), Gibbs free energy changes (ΔG^o) and entropy changes (ΔH^o) were studied on the formaldehyde adsorption process using the AC, AC/Fe_3O_4, CaO/Fe_3O_4 and AC/Fe_3O_4/CaO nanocomposite (Table 5). For all 4 adsorbents, ΔH^o value was negative, which implies that the uptake process using all adsorbents is exothermic. Also, the value of ΔS^o for all four adsorbents was negative, which indicates that the changes that happened in the adsorbents structure are not significant and the uptake process is physical. Moreover, the values of ΔG^o were negative, which shows that the uptake process in all the considered temperatures is favorable and spontaneous. Furthermore, the value of ΔG^o increased with increasing temperature, indicating that at low temperatures, the sorption process is more favorable and this was also observed in investigating the impact of temperature on the uptake efficiency. All in all, the examined thermodynamic parameters demonstrate that the aforementioned adsorbents can be used in the formaldehyde uptake process without needing any input energy and are suitable for commercial applications [42].

6. Sorption/Desorption Study and the Effect of Interfering Ions

The reusability of an adsorbent is a critical factor in its ability to be industrialized and this parameter was evaluated for the AC, AC/Fe_3O_4, CaO/Fe_3O_4 and AC/Fe_3O_4/CaO. To do so, the solution containing H_2SO_4 with different concentrations was examined (Fig. 11(a)). As seen, the desorption percentage of formaldehyde using all adsorbents increased with increasing the concentration of H_2SO_4, but this increase intensified to a concentration of 2 molar but after that, it was not significant. Then, to examine the desorption capability and the reusability of the four adsorbents, a 2 molar H_2SO_4 solution was used (Fig. 11(b)).

As can be seen, the adsorption percentage of formaldehyde decreased using all adsorbents with increasing the adsorption/desorption steps, which can be due to the damage and changes that happened on the mentioned adsorbents' surfaces during the sorption/desorption process. But as can be seen, the reduction in the sorption percentage was small for all adsorbents. For AC, the reduction in the sorption percentage after five cycles was approximately 7% (from 94.34% to 87.54%), but for AC/Fe_3O_4 (from 95.24% to 91.34%) and AC/CaO/Fe_3O_4 (from 97.67% to 93.82%), this value is less than 5%. Also, the reduction in the adsorption efficiency for CaO/Fe_3O_4 composite after five cycles was 5.6% (from 94.85 to 89.54%). These findings show that all adsorbents have high reusability for formaldehyde sorption. The outcomes show that the use of CaO and Fe_3O_4 nanoparticles increases the reusability of the adsorbents, in addition to the increase in the sorption capacity observed in the previous sections.

There are various ions in wastewater that sometimes compete with the considered pollutant molecules and affect the uptake efficiency. These ions have an interfering effect on the uptake process [62]. To investigate the competition between these ions and formaldehyde for adsorption on the surface of adsorbents, solutions containing formaldehyde and carbonate, sulfate, nitrate, and chloride ions were prepared. The impact of interfering ions on the uptake of formaldehyde from water is illustrated in Fig. 11(c). As

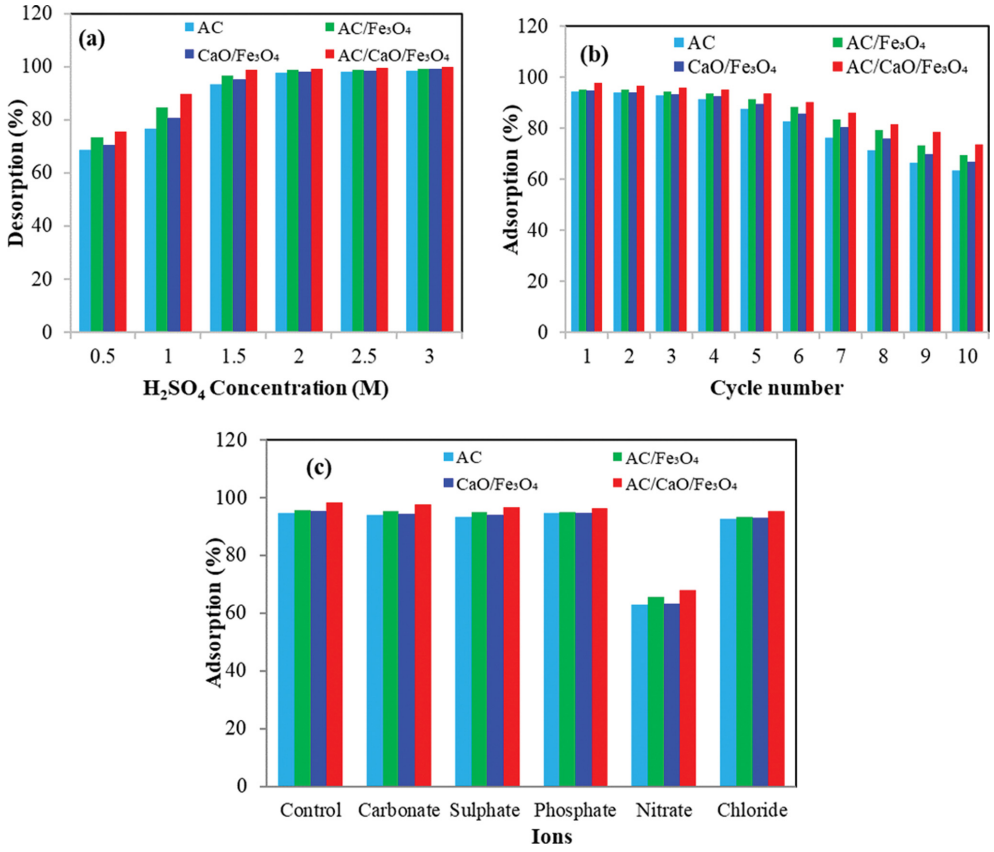

Fig. 11. The impact of H_2SO_4 concentration on the formaldehyde desorption from the surface of the AC, AC/Fe_3O_4, CaO/Fe_3O_4 and AC/Fe_3O_4/CaO (a), the reusability of the adsorbents in the elimination efficiency of formaldehyde (b) and the impact of interfering ions on the uptake efficiency of formaldehyde (c).

can be seen, all these ions, except for nitrate, have almost little competition with formaldehyde to the extent that the reduction in the sorption percentage of formaldehyde in their presence is less than 3%. However, competition between nitrate ions and formaldehyde to be placed on the adsorbents surface has led to a 30% reduction in the sorption efficiency of formaldehyde, which may be due to the ionic interaction mechanism between nitrate and formaldehyde [63] and also the electrostatic interactions of nitrate ions with the given adsorbents.

Generally, the reusability of the aforementioned adsorbents was studied after ten cycles of reuse and the results show that these four adsorbents have significant reusability. Also, the impact of interfering ions (e.g., carbonate, sulphate, phosphate, nitrate, and chloride) shows that all these compounds except for nitrate, had almost little competition with formaldehyde ion.

CONCLUSION

Formaldehyde is a toxic and carcinogenic compound found in different concentrations in industrial wastewaters. In the present study, the activated carbon produced from date seeds was modified by Fe_3O_4 nanoparticles and calcium oxide and then used to study the sorption process of formaldehyde from aquatic solutions. The physical features of all the adsorbents (AC, AC/Fe_3O_4, CaO/Fe_3O_4 and AC/CaO/Fe_3O_4 nanocomposite) were studied through FT-IR, XRD, SEM, EDX, Map, VSM, BET and TEM analyses. The results showed that the optimized conditions for AC and AC/Fe_3O_4 composite were pH of 7, sorbent dosage of 3 g/L, contact time of 100 min, initial concentration of 5 mg/L, and temperature of 25 °C. Also, the optimized conditions for the sorption of formaldehyde using the AC/Fe_3O_4/CaO nano-composite were pH of 7, sorbent dosage of 2.5 g/L, contact time of 80 min, initial concentration of 5 mg/L, and temperature of 25 °C. According to the outcomes obtained from equilibrium and kinetic studies, the Freundlich isotherm model and pseudo-1st-order kinetic model were suitable to describe the uptake process using the AC. Also, the outcomes showed that the formaldehyde sorption process using the AC/Fe_3O_4 and CaO/Fe_3O_4 follows the Langmuir isotherm model and pseudo-2nd-order kinetic model. Furthermore, the formaldehyde sorption process using the AC/Fe_3O_4/CaO magnetic composite follows the Freundlich isotherm model and pseudo-2nd-order kinetic model. Moreover, the thermodynamic behavior of the formaldehyde sorption process using the adsorbents showed that the uptake process is spontaneous and exothermic. The findings also proved that modifying the activated carbon by magnetic nanoparticles and calcium oxide has led to the ease of separation, decrease in the process costs, and increase in the formaldehyde sorption efficiency. The high reusability of these four adsorbents proves their suitability for the industrial application of formaldehyde removal.

CONFLICT OF INTEREST

We have no conflict of interest to declare.

AUTHORS' CONTRIBUTIONS

All authors have contributed to the writing and reading of the manuscript. Experimental works were done by Hossein Khaleghi (Ph.D. student). Dr. Neemat Jaffarzadeh and Dr. Hossein Esmaeili were the supervisors and Dr. Bahman Ramavandi was the advisor. The manuscript was written by Mr. Hossein Khaleghi and Dr. Hossein Esmaeili. The manuscript was revised by Dr. Hossein Esmaeili, Dr. Neemat Jaffarzadeh and Dr. Bahman Ramavandi.

REFERENCES

1. Y. Chen, L. He, J. Li and S. Zhang, *Comput. Chem. Eng.*, **109**, 216 (2018).
2. L. He, Y. Chen and J. Li, *Resour. Conserv. Recycl.*, **133**, 206 (2018).
3. Y. Zvulunov, Z. Ben-Barak-Zelas, A. Fishman and A. Radian, *Chem. Eng. J.*, **374**, 1275 (2019).
4. D. Paliulis, *Pol. J. Environ. Stud.*, **25**, 251 (2016).
5. S. Arsawiset and S. Teepoo, *Analytica Chim. Acta*, **1118**, 63 (2020).
6. H. Wang, T. Song, Z. Li, J. Qiu, Y. Zhao, H. Zhang and J. Wang, *ACS Appl. Mater. Interfaces*, **13**, 25918 (2021).
7. X. Wang, Z. Feng, B. Xiao, J. Zhao, H. Ma, Y. Tian, H. Pang and L. Tan, *Green Chem.*, **22**, 6157 (2020).
8. F. Bahador, R. Foroutan, H. Esmaeili and B. Ramavandi, *Carbohydr. Polym.*, **251**, 117085 (2021).
9. T. Zhang, X. Wu, S. M. Shaheen, J. Rinklebe, N. S. Bolan, E. F. Ali, G. Li and D. C. Tsang, *J. Hazard. Mater.*, **416**, 125738 (2021).
10. K. Vellingiri, K. Vikrant, V. Kumar and K. H. Kim, *Chem. Eng. J.*, **399**, 125759 (2020).
11. X. Zhu, X. Gao, R. Qin, Y. Zeng, R. Qu, C. Zheng and X. Tu, *Appl. Catal. B Environ.*, **170**, 293 (2015).
12. X. Zhang, X. Sun, T. Lv, L. Weng, M. Chi, J. Shi and S. Zhang, *J. Mater. Sci. Mater. Electron.*, **31**, 13344 (2020).
13. D. Yuan, L. Tian, D. Gu, X. Shen, L. Zhu, H. Wu and B. Wang, *J. Clean. Prod.*, **156**, 310 (2017).
14. R. Darvishi Cheshmeh Soltani, A. Rezaee, M. Safari, A. R. Khataee and B. Karimi, *Desalin. Water Treat.*, **53**, 1613 (2015).
15. B. Xing, G. Yang, H. Chen and X. Liu, *React. Kinet. Mech. Catal.*, **126**, 547 (2019).
16. A. Talaiekhozani, M. Salari, M. R. Talaei, M. Bagheri and Z. Eskandari, *J. Environ. Manage.*, **184**, 204 (2016).
17. M. Sarabadan, H. Bashiri and S. M. Mousavi, *Korean J. Chem. Eng.*, **36**, 1575 (2019).
18. F. Mahmoodi, P. Darvishi and B. Vaferi, *J. Iran. Chem. Soc.,* **15**, 2747 (2018).
19. C. Ma, X. Zhang, K. Wen, R. Wang and R. Han, *Korean J. Chem. Eng.*, **38**, 135 (2021).
20. J. E. T. Tech, *J. Environ. Treat. Tech.*, **2**, 12 (2014).
21. K. Wang, J. Zhao, H. Li, X. Zhang and H. Shi, *J. Taiwan Inst. Chem. Eng.*, **61**, 287 (2016).
22. A. Khamkeaw, M. Phisalaphong, B. Jongsomjit, K. Y. A. Lin and A. C. Yip, *J. Hazard. Mater.*, **384**, 121161 (2020).
23. M. Salman, M. Athar, U. Shafique, R. Rehman, S. Ameer, S. Zulfiqar Ali and M. Azeem, *Turkish J. Eng. Environ. Sci.*, **36**, 263 (2012).
24. J. P. Bellat, G. Weber, I. Bezverkhyy and J. F. Lamonier, *Micropor. Mesopor. Mater.*, **288**, 109563 (2019).
25. J. P. Bellat, I. Bezverkhyy, G. Weber, S. Royer, R. Averlant, J. M. Giraudon and J. F. Lamonier, *J. Hazard. Mater.*, **300**, 711 (2015).
26. C. Ma, X. Zhang, K. Wen, R. Wang and R. Han, *Korean J. Chem. Eng.*, **38**, 135 (2021).
27. I. Syafiqah and H. W. Yussof, *Water Conserv. Manag.*, **2**, 10 (2018).
28. K. Seffati, H. Esmaeili, B. Honarvar and N. Esfandiari, *Renew. Energy*, **147**, 25 (2020).
29. A. Alsultan, A. Mijan and Y. H. Taufiq-Yap, *Mater. Sci. Forum*, **840**, 348 (2016).
30. T. H. Liou, P. Y. Wang and Y. H. Liou, *BioResources*, **11**, 6110 (2016).
31. C. Zhou, D. Ding, W. Zhu, X. Chang, T. Zhang, H. Wu, H. Yang and L. Sun, *Appl. Surf. Sci.*, **520**, 146324 (2020).
32. T. Takada, *Nano Biomedicine*, **3**, 282 (2011).
33. L. Wang, Y. Wu, S. Liu, Y. Zhang, Y. Chen, H. Ma, Z. Zhu and J. Zhou, *BioResources*, **14**, 7193 (2019).
34. L. He, Y. Chen, H. Zhao, P. Tian, Y. Xue and L. Chen, *Sci. Total Environ.*, **627**, 1585 (2018).
35. X. Cheng, L. He, H. Lu, Y. Chen and L. Ren, *J. Hydrol.*, **540**, 412 (2016).
36. M. M. Boushehrian, H. Esmaeili and R. Foroutan, *J. Environ. Chem. Eng.*, **8**, 103869 (2020).
37. N. Bougdah, N. Messikh, S. Bousba, F. Djazi, P. Magri and M. Rogalski, *Curr. Res. Green Sustain. Chem.*, **3**, 100038 (2020).
38. F. Takmil, H. Esmaeili, S. M. Mousavi and S. A. Hashemi, *Adv. Powder Technol.*, **31**, 3236 (2020).
39. H. Esmaeili, R. Foroutan, D. Jafari and M. A. Rezaei, *Korean J. Chem. Eng.*, **37**, 804 (2020).
40. A. Yildirim and Y. Bulut, *Environ. Technol. Innov.*, **17**, 100560 (2020).
41. Z. Keshtkar, S. Tamjidi and B. Vaferi, *Environ. Technol. Innov.*, **22**, 101439 (2021).
42. A. Ahmadi, R. Foroutan, H. Esmaeili and S. Tamjidi, *Environ. Sci. Pollut. Res.*, **27**, 14044 (2020).
43. M. C. G. Albuquerque, D. C. S. Azevedo, C. L. Cavalcante Jr., J. Santamaria-Gonzalez, J. M. Merida-Robles, R. Moreno-Tost, E. Rodriguez-Castellon, A. Jimenez-Lopez and P. Maireles-Torres, *J. Mol. Catal. A Chem.*, **300**, 19 (2009).
44. A. A. Mousavi, C. Zhang, S. F. Masri and G. Gholipour, *Struct. Health Monit.* (2021).
45. S. Yao, J. Zhang, D. Shen, R. Xiao, S. Gu, M. Zhao and J. Liang, *J. Colloid Interface Sci.*, **463**, 118 (2016).
46. Z. Wang, M. Zhong and L. Chen, *Desalin. Water Treat.*, **57**, 13225 (2016).
47. L. Zhang, M. Zhang, S. You, D. Ma, J. Zhao and Z. Chen, *Sci. Total Environ.*, **780**, 146505 (2021).
48. A. R. Bagheri, M. Ghaedi, A. Asfaram, A. A. Bazrafshan and R. Jannesar, *Ultrason. Sonochem.*, **34**, 294 (2017).
49. Z. Ni, X. Cao, X. Wang, S. Zhou, C. Zhang, B. Xu and Y. Ni, *Coatings*, **11**, 749 (2021).
50. F. Taghizadeh, M. Ghaedi, K. Kamali, E. Sharifpour, R. Sahraie and M. K. Purkait, *Powder Technol.*, **245**, 217 (2013).
51. M. Zhang, L. Zhang, S. Tian, X. Zhang, J. Guo, X. Guan and P. Xu, *Chemosphere*, **253**, 126638 (2020).

52. S. Ghanbari and B. Vaferi, *Acta Astronaut.*, **112**, 19 (2015).
53. S. Arivoli, M. Hema, S. Parthasarathy and N. Manju, *J. Chem. Pharm. Res.*, **2**, 626 (2010).
54. K. Zhang, Q. Huo, Y. Y. Zhou, H. H. Wang, G. P. Li, Y. W. Wang and Y. Y. Wang, *ACS Appl. Mater. Interfaces*, **11**, 17368 (2019).
55. L. Zhang, J. Zheng, S. Tian, H. Zhang, X. Guan, S. Zhu, X. Zhang, Y. Bai, P. Xu, J. Zhang and Z. Li, *J. Environ. Sci.*, **91**, 212 (2020).
56. B. Vaferi, M. Bahmani, P. Keshavarz and D. Mowla, *J. Environ. Chem. Eng.*, **2**, 1252 (2014).
57. B. Li, H. Wu, C. Zhang, W. Zheng, D. Sun and S. Lei, *Desalin. Water Treat.*, **165**, 148 (2019).
58. R. Prasad and K. D. Yadav, *Water Conserv. Manag.*, **4**, 83 (2021).
59. N. S. Zafisah, W. L. Ang and A. W. Mohammad, *Water Conserv. Manag.*, **2**, 5 (2018).
60. A. Mohseni-Bandpi, T. J. Al-Musawi, E. Ghahramani, M. Zarrabi, S. Mohebi and S. Abdollahi Vahed, *J. Mol. Liq.*, **218**, 615 (2016).
61. H. Esmaeili and S. Tamjidi, *Environ. Sci. Pollut. Res.*, **27**, 31652 (2020).
62. M. R. Awual, M. Khraisheh, N. H. Alharthi, M. Luqman, A. Islam, M. R. Karim, M. M. Rahman and M. Abdul Khaleque, *Chem. Eng. J.*, **343**, 118 (2018).
63. H. T. Banu and S. Meenakshi, *J. Water Process Eng.*, **16**, 81 (2017).